Supporting Information for:

Edge fires drive the shape and stability of tropical forests

L. Hébert-Dufresne[a,b], A. F. A. Pellegrini[c,d], U. Bhat[b,e,f], S. Redner[b], S. W. Pacala[d], A. Berdahl[b,g]

[a]*Department of Computer Science and Vermont Complex Systems Center, University of Vermont, Burlington, VT 05405, USA*

[b]*Santa Fe Institute, Santa Fe, NM, 87501, USA*

[c]*Department of Earth System Science, Stanford University, Stanford, CA 94305, USA*

[d]*Department of Ecology & Evolutionary Biology, Princeton University, Princeton, NJ, 08544, USA*

[e]*Department of Physics, Boston University, Boston, MA 02215, USA*

[f]*School of Natural Sciences, University of California, Merced, Merced, CA 95343, USA*

[g]*School of Aquatic and Fishery Sciences, University of Washington, Seattle, WA 98195, USA*

Appendix A. Study area

We restricted our study to protected areas in the Brazilian Cerrado. Please see Fig. A.1 for a map.
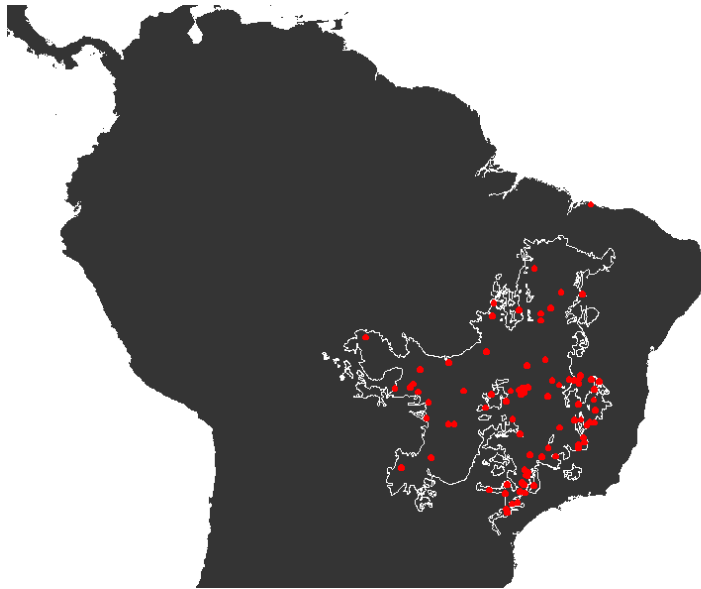

Figure A.1: Map of study areas. Outline on map demarks the Cerrado. Study areas are coloured red.

Appendix B. Rainfall and tree cover distribution in the Cerrado

The distribution of annual rainfall [1] per forest patch in the Cerrado is given in Fig. B.2. The distribution lends itself well to a distinction in terms of 3 different climates: forests receiving less than 1100 mm, between 1100 and 1800 mm and more than 1800 mm.

The distribution of tree cover over our study region is given in Fig. B.3. Unlike the distribution of rainfall, there is no clear threshold separating obvious forests sites from obvious grassland sites. Thankfully, the two most common tree cover values are 0 and 100%. For sites with an intermediate value, we use thresholds of 50% and 75% to either include or exclude the local maximum around 55 and 60%.

As shown in Fig. B.4, some areas in our study region are dominated by geographical features. However, numerically, the bulk of the data comes from grass-forest mosaics as shown in Fig. 1 of the main text.
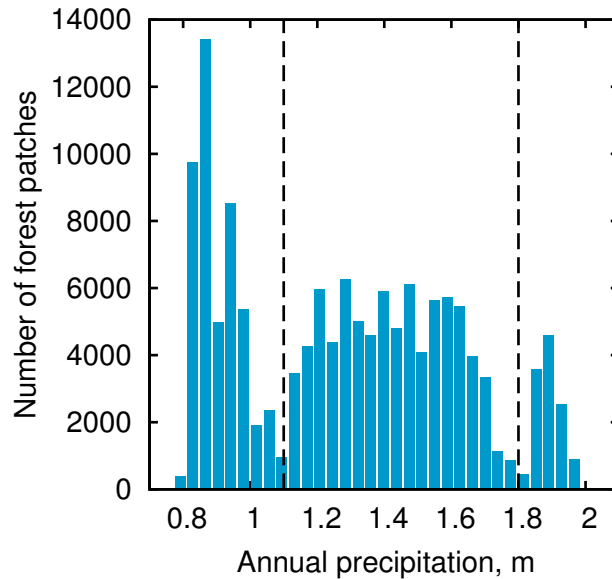

Figure B.2: Histogram of annual precipitation. The *y*-axis shows the number of forest patches in our remotely sensed data set that have a specific annual rain fall. The dashed vertical line demark the boundaries between sites with low, medium and high rain fall, presented in Figure 1E&F of the main text.

Appendix C. Statistical estimates of scale exponents

The empirical data is characterized by two sets fat-tail distributions: the distribution functions $f(A)$ of forest area A, and the distribution functions $g(P)$ of perimeter P. The quantities A and P are themselves linked by a scaling relation of the form $P \sim A^\gamma$. Let $f(A) \sim A^{-\phi}$ and $g(P) \sim P^{-\theta}$ for large values of A and P, we can derive γ as a function of ϕ and θ. Doing so allows us to use the robust statistical framework developed to estimate scaling exponents in power-law distributions in order to also estimate γ, and obtain error bounds on all exponents.
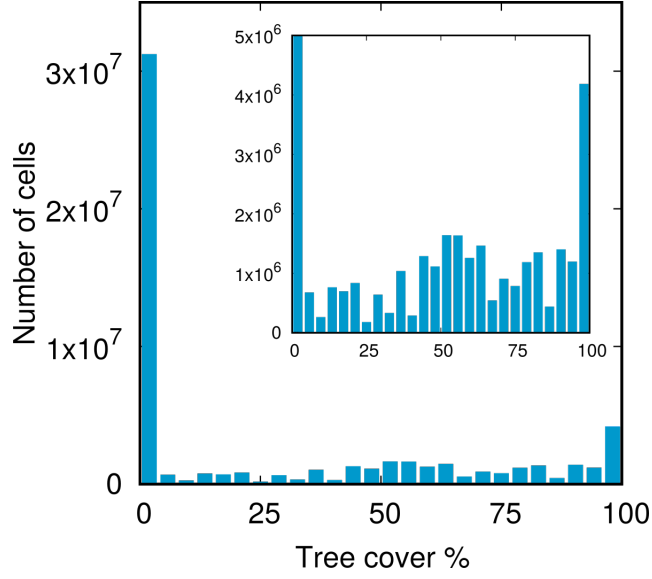
2

Figure B.3: Histogram of tree cover. The *y*-axis shows the number of sites in our remotely sensed data set that have a estimated tree cover. The inset uses a limited *y*-axis to highlight the distribution of tree cover among forested sites.
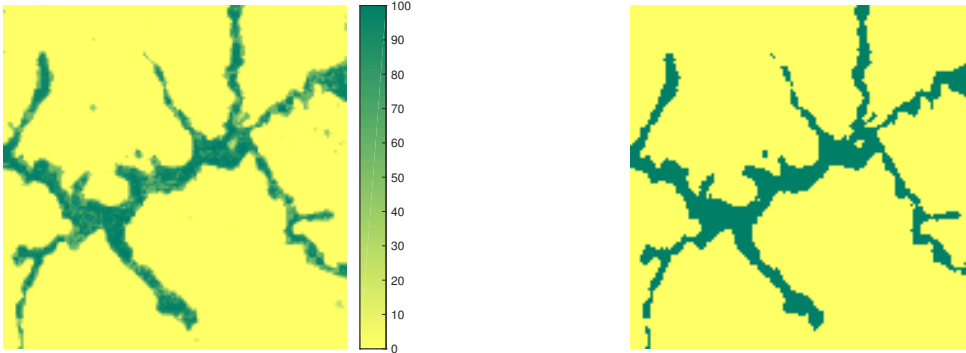

Figure B.4: Tree cover in an area where forest cover is strongly influenced by geographical features. Left panel shows raw data; right panel shows the same area with the 50% tree cover threshold applied. The panel show a 4 km by 4 km area.

First, let us derive the relation between γ, ϕ and θ. We have

$$g(P)dP = f(A(P))\frac{dA}{dP}dP \sim P^{-\phi/\gamma}P^{1/\gamma-1}dP \tag{C.1}$$

where we use both $f(A) \sim A^{-\phi}$ and the variable change $P \sim A^{\gamma}$ to rewrite $g(P)dP$. If we now use the correspondence between the last expression and $g(P) \sim P^{-\theta}$, we obtain

$$\gamma = \frac{\phi - 1}{\theta - 1} \ . \tag{C.2}$$

We can use Eq. C.2 to estimate γ if we can obtain estimates and error bounds on both ϕ and θ. To do so, we rely on the framework developed by Clauset, Shalizi and Newman [2], which we here summarize. With a sequence of

3

observations $X = \{x_i\}$, the likelihood that X came from the normalized discrete probability distribution $P(x)$ would be the product of the likelihood of every observation: $\prod_i P(x_i)$. The log-likelihood would then simply be

$$\mathcal{L}(P(X)) = \ln\left[\prod_i P(x_i)\right] = \sum_i \ln\left[P(x_i)\right] .$$

(C.3)

In our case, since the power-law behavior might only be present in the tail, we define the observed data as the subset of all n observations $x_i \geq x_{\min}$ where $x_{\min}$ is an appropriate bound for the power-law tail. Thus, the log-likelihood of data x_i depends on both ν and $x_{\min}$ following

$$\mathcal{L}(\nu, x_{\min}) = \ln\left[\prod_{i=1}^{n} \frac{x_i^{-\nu}}{\sum_{j>x_{\min}} j^{-\nu}}\right]$$

(C.4)

where the sum is simply the normalizing factor of the tail. This sum can be referred to as a generalized zeta function $\zeta(\nu, x_{\min})$. The MLE of ν and $x_{\min}$, usually noted $\hat{\nu}$ and $\hat{x}_{\min}$, are thus obtained by maximizing

$$\mathcal{L}(\nu, x_{\min}) = -n \ln\left[\zeta(\nu, x_{\min})\right] - \nu \sum_{i=1}^{n} \ln k_i .$$

(C.5)

Maximizing for ν using a given $x_{\min}$ is straightforward: we scan potential ν values, typically in steps of 10^{-2} or 10^{-3}. Choosing the right $x_{\min}$ is another story. If too low, we risk including the non-power-law behaviour (if any) of the data. If too high, we lose too many observations and the estimate of ν will also suffer. For consistency, we used $x_{\min} = 10$ (in pixels and square pixels, not meters and square meters) on all data, both simulated and empirical. The error bounds on ν are then given by the following standard deviation:

$$\sigma = \frac{\hat{\nu} - 1}{\sqrt{n}} + O(n) ,$$

(C.6)

where n is the number of data points above $\hat{x}_{\min}$.

Using this procedure in the three climatic regions and both the 50% and 75% forest cover threshold, we obtain the following intervals for the exponents

$$\gamma_{\text{high},50} = 0.68 \pm 0.03, \quad \gamma_{\text{medium},50} = 0.70 \pm 0.01, \quad \gamma_{\text{low},50} = 0.70 \pm 0.02 ;$$
$$\phi_{\text{high},50} = 1.78 \pm 0.02, \quad \phi_{\text{medium},50} = 1.81 \pm 0.01, \quad \phi_{\text{low},50} = 1.94 \pm 0.02 ;$$
$$\theta_{\text{high},50} = 2.15 \pm 0.02, \quad \theta_{\text{medium},50} = 2.15 \pm 0.01, \quad \theta_{\text{low},50} = 2.35 \pm 0.02 .$$

$$\gamma_{\text{high},75} = 0.66 \pm 0.03, \quad \gamma_{\text{medium},75} = 0.70 \pm 0.02, \quad \gamma_{\text{low},75} = 0.71 \pm 0.01 ;$$
$$\phi_{\text{high},75} = 1.79 \pm 0.02, \quad \phi_{\text{medium},75} = 1.84 \pm 0.01, \quad \phi_{\text{low},75} = 1.84 \pm 0.01 ;$$
$$\theta_{\text{high},75} = 2.20 \pm 0.02, \quad \theta_{\text{medium},75} = 2.20 \pm 0.01, \quad \theta_{\text{low},75} = 2.47 \pm 0.01 .$$

Note that the error on ϕ and θ values are theoretical standard error, whereas error on the γ values correspond to 95% intervals obtained using all values of ϕ and θ within 1.96 standard deviations of their respective mean (we assume normality considering the possible values γ are bounded).

While the intervals do not overlap for ϕ and θ across all climatic regions, the estimates for γ are surprisingly robust. We find similar values in our simulated data, shown in Table 2 of the main text, such that almost all intervals of confidence overlap at least around 0.69. In the main text, we reported the average maximum-likelihood value as an averaged 95% interval.
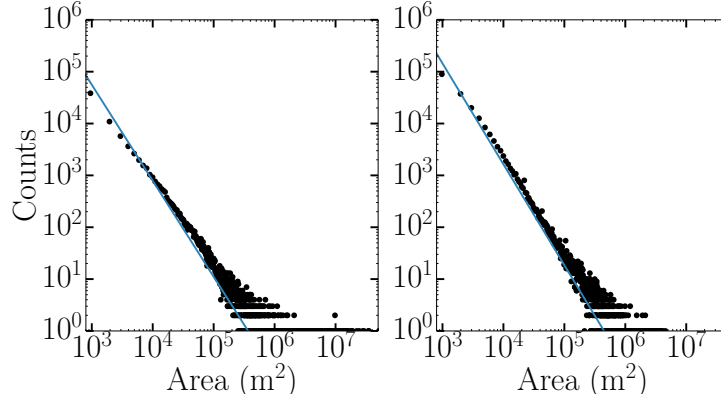

Figure C.5: Example of the fits obtained on two forest area distributions: Empirical data from the medium range of precipitation using the 50% tree cover threshold (left) and data from the simulation set using a 515x512 lattice, $p_\lambda = 0.1$, $p_\alpha = 0.004$, $p_\beta = 10^{-5}$, $p_f = 4 \cdot 10^{-7}$, $p_G = 0.9$ and $p_T = 0.1$. (right). The scaling exponents obtained are, respectively, 1.81 and 1.95.

Appendix D. Additional flow results

One of our main results concern our ability to predict the fate of individual forest patches based on their current shape. We here revisit the analysis behind Fig. 2 in the main text using a different set of parameters. In Fig. D.6, we find that flows of forest patches in the perimeter-area space appear robust to changes in parameters. The simulations done for this version use a 256x256 lattice with $p_\lambda = 0.1$, $p_\alpha = 0.022$, $p_\beta = 10^{-6}$, $p_f = 3.4 \cdot 10^{-6}$, $p_G = 0.9$ and $p_T = 0.1$. Flows are now averaged over 50 time steps.

Appendix E. Coarse-graining

The empirical data was constructed by coarse-graining satellite imagery according to the size of the tree cover (less or more than 50% tree cover for savanna-grassland or forest respectively). This coarse-graining process obviously affects the shape of a forest, but to what extent? Empirical results tell us that these regions are typically separated in areas of low (<50%) or high (>75%) tree cover. Consequently, any threshold between 50-75% is reasonable, and we used 50% following other sources in the literature.

However, we can take the analysis a step further and coarse-grain our numerical simulations following the same process. We group sites of our lattices in pixels of 4 original sites (2x2) to which we assign a "forest" state if 2 or more sites in the pixel are in a true "forest" site. This coarse-graining process thus follows the same 50% threshold to distinguish between forest and grassland.

In Fig. E.7, we present results obtained by first running our entire numerical methodology on our model using a 256×256 square lattice, with $p_\lambda = 10^{-1}$, $p_\beta = 10^{-4}$, $p_\alpha = 5 \cdot 10^{-3}$, $\rho_G = 0.9$, $\rho_T = 0.1$ and $p_f = 1.25 \cdot 10^{-5}$; then by applying this coarse-graining process. We find that the same scaling relation fits both the original data, and coarse-grained data.
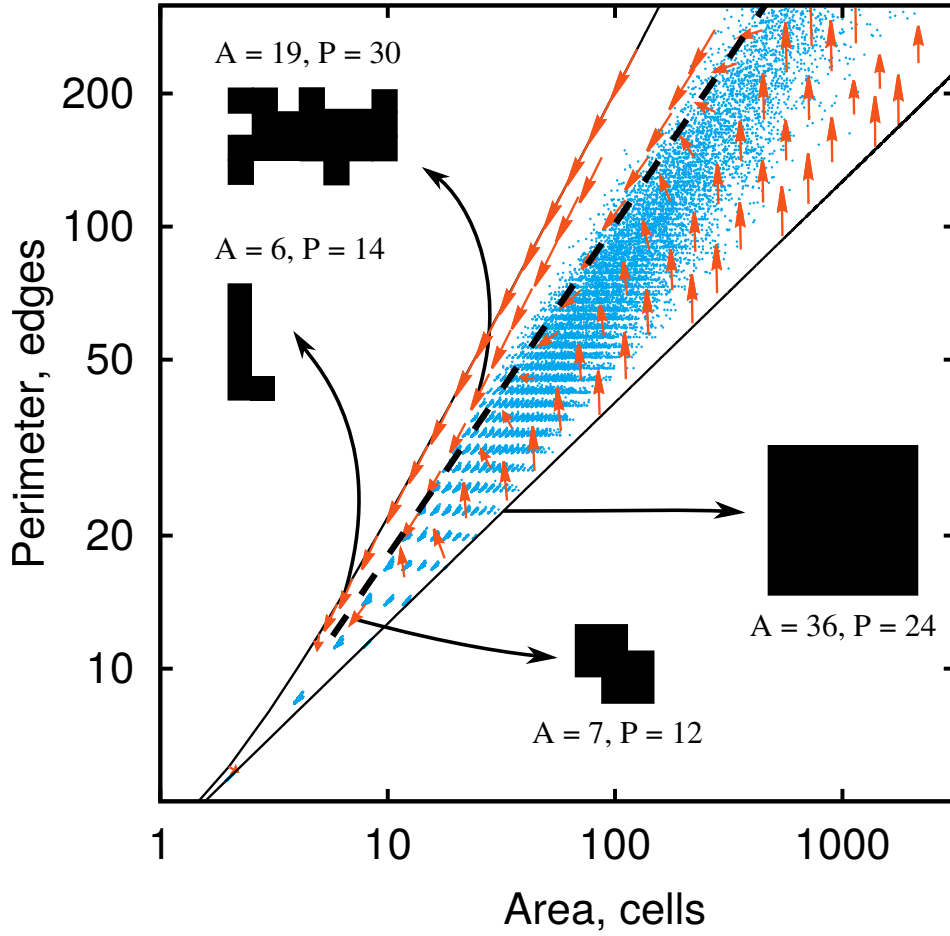
Figure D.6: This figure validates the robustness of Fig. 2 in the main text to model parameters.

Appendix F. Linear scaling in previous models, and in the case $\alpha \to 0$

Recent models of fire in forest-grassland system (e.g. [3]) focused on the bistability of the system and not on the spatial organization. Consequently, they do not incorporate a local mechanism for tree spreading (our p_α parameter). Indeed, we do find a large region of bistability (first order transition) in the limit $p_\alpha \to 0$. However, in this limit, the system does not reproduce the correct scaling of perimeter to area for individual forest patches, and consequently models in this regime can not inform policy at the local level. We present results supporting this claim in Fig. F.8.

Appendix G. Details of the mean-field analysis

We write the mean-field equations for the spatial simulation as follows. Define the normalized densities of grass, trees, ash and burning entities (both grass and trees can be lumped together, as the fire propagation rate is independent of which entity catches fire in our model) as a function of time as $G(t)$, $T(t)$, $A(t)$ and $B(t)$. To derive the mean-field
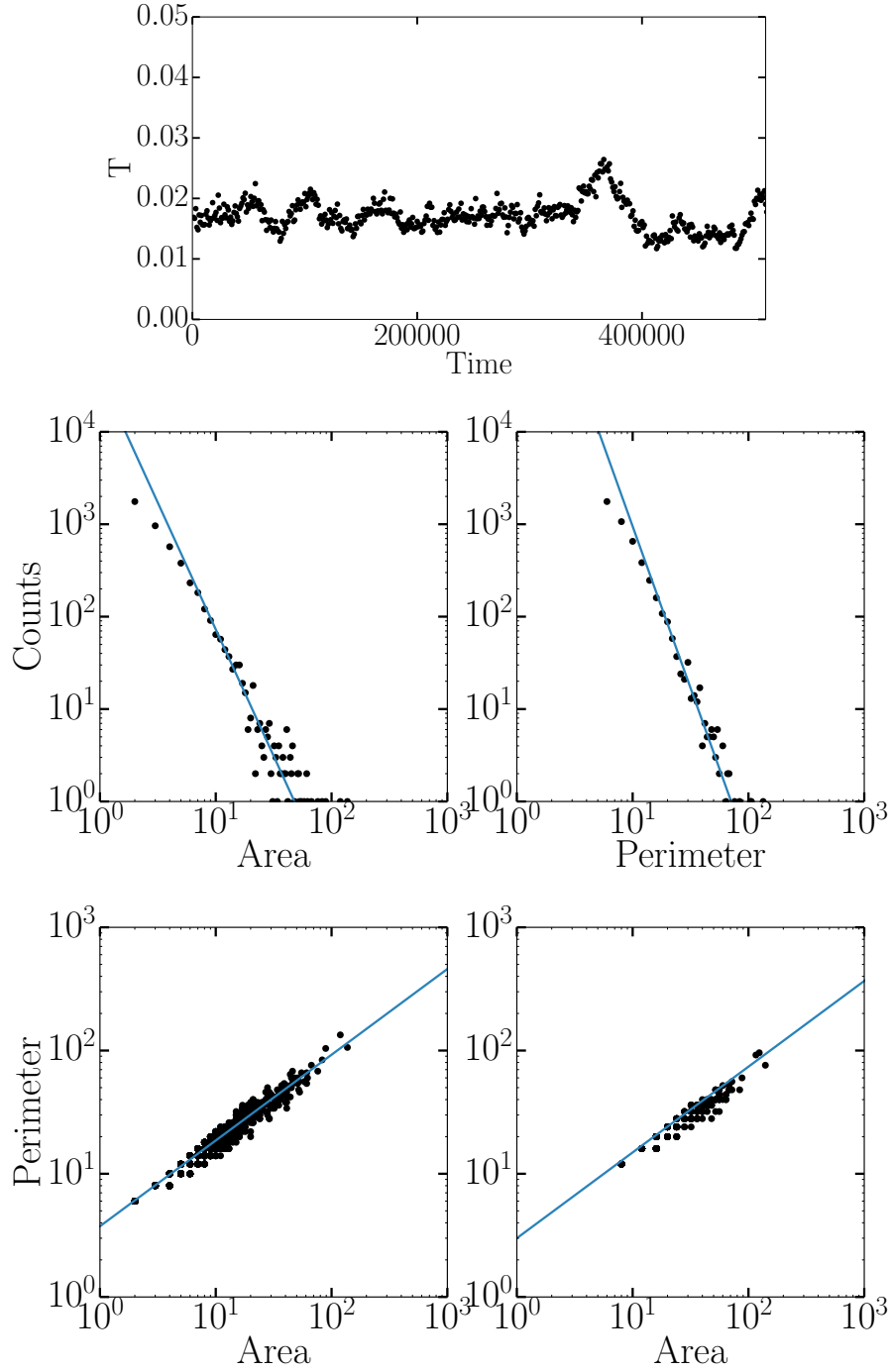
Figure E.7: (top figure) Time series of the total fraction of forested sites T as a function of time. One time step correspond to one iteration of the rules of our model over all lattice sites. We observe the system at every 1000 time steps. (middle row) Histogram of area and perimeter for every forest cluster observed. The estimated scaling exponents are shown in blue. (bottom row) Our analysis leads to a relation of perimeter to area following a scaling exponent of 0.696 (95% confidence interval [0.62, 0.78]) which fits the data well both before (left) and after (right) the coarse-graining process. To plot the coarse-grained data, we multiplied area by 4 and perimeter by 2 (so that their units still match that of the right plot).
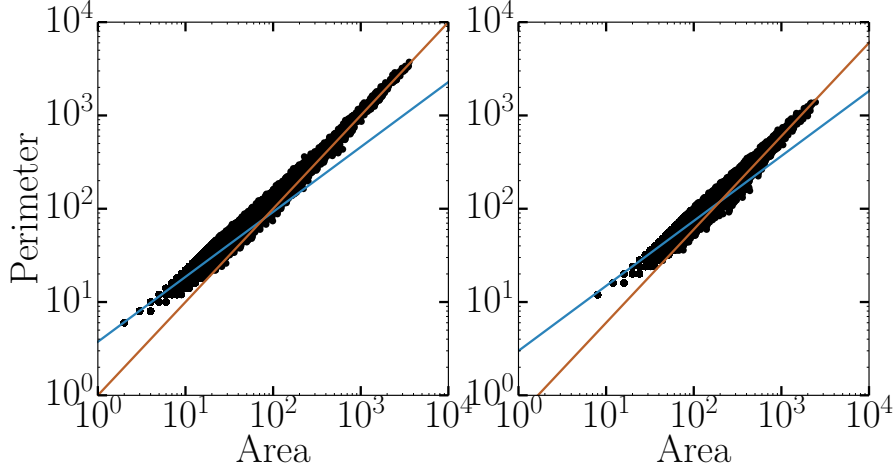
Figure F.8: Results obtained on a 256×256 square lattice, using $p_\lambda = 10^{-2}$, $p_\beta = 2 \cdot 10^{-3}$, $\rho_G = 0.9$, $\rho_T = 0.1$ with (left) $p_f = 3 \cdot 10^{-4}$ and $p_\alpha = 0$ or (right) $p_f = 5 \cdot 10^{-4}$ and $p_\alpha = 10^{-4}$. The scaling of perimeter appears closer to a linear relation (orange line) rather than the correct 0.7 power law (blue line). While the linear fit is not excellent on the right figure, our fitting procedure suggests a scaling with exponent 0.95 (95% confidence interval [0.84, 1.09]).

equations, we first assign every site ij on the square two-dimensional lattice with the Bernoulli random variables $G_{i,j}(t)$, $T_{i,j}(t)$, $A_{i,j}(t)$, and $B_{i,j}(t)$. At each site, only one of these four random variables can take the value 1, while the remaining three variables are equal to 0.

We now write the probability for a particular random variable to undergo a change. Based on the elemental steps of the model that were enumerated in the main text, the change in the probability that a site contains a grass patch in a time increment Δt is given by,

$$\Delta G_{i,j} = \lambda \Delta t A_{i,j} - G_{i,j} \Delta t \left[\beta + f + \sum_{(k,\ell) \in \mathcal{N}(i,j)} (\rho_G B_{k,\ell} + \alpha T_{k,\ell}) \right], \tag{G.1}$$

where $\mathcal{N}(i,j)$ denotes the nearest-neighborhood of site (i,j). Analogous equations can be written for the change in the probabilities that the site is occupied by a tree, by ash, or that the site is burning.

We then apply the expectation operator to all the quantities and make the following mean-field assumptions,

1. The lattice is translationally invariant implying $\langle G_{i,j} \rangle$ is independent of (i,j)
2. That averages of two-body quantities, such as $\langle GT \rangle = \langle G \rangle \langle T \rangle$, etc.

These assumption lead to the following set of rate equations:

$$\begin{aligned}
\dot{G} &= \lambda A - (\beta + f) G - 4\rho_G BG - 4\alpha GT, \\
\dot{T} &= 4\alpha T (G + A) + \beta G - 4\rho_T BT, \\
\dot{A} &= \mu B - \lambda A - 4\alpha TA, \\
\dot{B} &= fG + 4\rho_G BG + 4\rho_T BT - \mu B.
\end{aligned} \tag{G.2}$$

We can solve (G.2) numerically for different parameter values. Here ρ_G and ρ_T are simply related to p_G and p_T, the probabilities that a grass (or tree) patch that neighbors a burning patch catches fire before the burning patch turns to ash. In particular ρ_G is related to p_G by $p_G = \rho_G/(\rho_G + r)$, which implies that $\rho_G = r p_G/(1 - p_G)$. Similarly $\rho_T = r p_T/(1 - p_T)$. We fix $p_G = 0.9$ and $p_T = 0.1$, as used in the simulations, but in general p_G, the probability that fire

spreads to a grass patch, is large and p_T, the probability that fire spreads to a tree patch, is small. Then we fix $\lambda = 0.05$, equivalently fixing the time units. We choose a set of values for α from 0 to $\lambda/10$ (since trees grow much slower than grass) and different values for β. For each (α, β), we find T^*, the steady state density of trees as a function of the fire rate f. As we see in Fig. G.9, (G.2) exhibits rich behavior and corresponds to what we observe in the simulations. For small values of β, the system undergoes a first-order transition in the tree density as a function of the fire rate and consequently shows hysteresis. For large values of β, the system undergoes a second-order transition in the tree density. The critical value of β_c decreases as a function of α (Fig. G.10). There also exists a value α_c beyond which $T^* = 1$ is stable for any value of f and the fully forested state is *always* the only stable solution of the system.
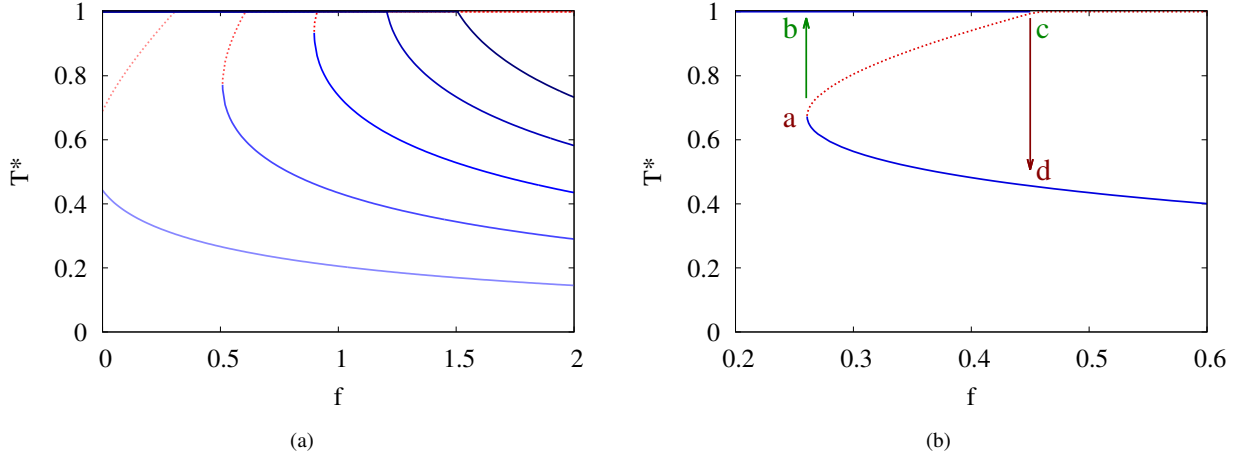

(a)

(b)

Figure G.9: (a) Fixed point value of T, for $\alpha = 0.001$ and $\beta = 0.2, 0.4, \cdots, 1.0$ as a function of f. Stable and unstable solutions are in blue (solid) and red (dashed) lines respectively. $\beta_c \approx 0.7$ (b) Bistable region for $\alpha = 0.001$ and $\beta = 0.3$.
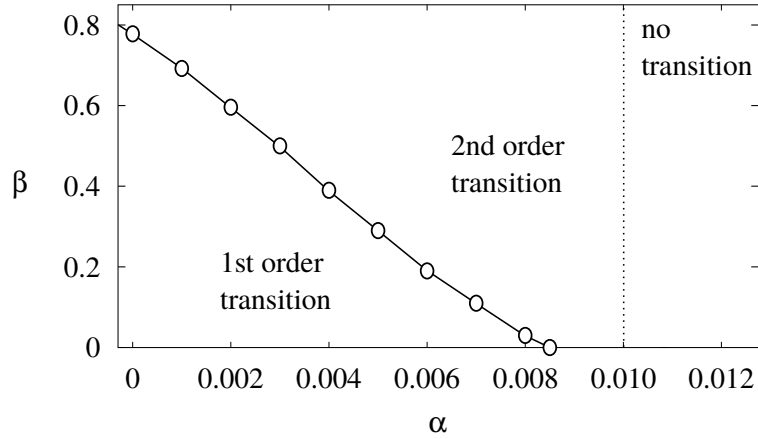

Figure G.10: Diagram of the possible phase transition. The markers follow β_c as a function of α; β_c is the value of β that divides the first- and second-order transitions in T^* as a function of f. The vertical dotted line marks α_c, which is the value of α beyond which $T^* = 1$ is stable even for infinite f. These results were obtained with $\lambda = 0.05$, $p_t = 0.1$ and $p_g = 0.9$.

Appendix H. Derivation of α_c, where a fully-forested state is the only outcome

Our mean-field results indicated that there exists a value α_c above which there are no phase transitions in f; i.e., $T^* = 1$ is stable even for infinite fire rates f. To derive this value in a simpler way, we can write the Jacobian for

Eq. (G.2) and find the value of α, above which all the eigenvalues of the Jacobian at $T = 1$ are negative, for all values of f and β. We use the fact that $G + T + A + B = 1$ and write the Jacobian of the reduced system with just the variables G, T and A and substitute $B = 1 - G - T - A$. We evaluate the Jacobian at $(G, T, A) = (0, 1, 0)$ to obtain,

$$
J = \begin{bmatrix}
-\beta - f - 4\alpha & 0 & \lambda \\
4\alpha + \beta + 4\rho_T & 4\rho_T & 4\alpha + 4\rho_T \\
-\mu & -\mu & -\mu - \lambda - 4\alpha
\end{bmatrix}
\tag{H.1}
$$

which can then be evaluated in the limit $f \to \infty$ with $\beta = 0$ for simplicity. Again, α_c is the smallest α for which all eigenvalues are negative in the limit $f \to \infty$. Numerically, we find that for $\alpha > \alpha_c = 0.01$, $T = 1$ is always a steady state.

[1] R. J. Hijmans, S. E. Cameron, J. L. Parra, P. G. Jones, A. Jarvis, *International journal of climatology* **25**, 1965 (2005).
[2] A. Clauset, C. R. Shalizi, M. E. Newman, *SIAM review* **51**, 661 (2009).
[3] E. Schertzer, A. Staver, S. Levin, *Journal of Mathematical Biology* **70**, 329 (2015).